Quantitative Analysis of Adsorbate Induced Segregation at Bimetallic Surfaces: Improving the Accuracy of Medium Energy Ion Scattering Results

Christopher J Baddeley,*,†,‡ Lucy H Bloxham,† Sylvie C Laroze,† Rasmita Raval,†,§ Timothy CQ Noakes,|| and Paul Bailey||

Leverhulme Centre for Innovative Catalysis, Department of Chemistry, University of Liverpool, Liverpool, United Kingdom L69 7ZD, Surface Science Research Centre, University of Liverpool, Liverpool, United Kingdom L69 3BX, and Medium Energy Ion Scattering Facility, CLRC Daresbury Laboratory, Daresbury, United Kingdom WA4 4AD

Received: September 13, 2000; In Final Form: December 15, 2000

Bimetallic systems respond dynamically to the nature of the gas phase in contact with the surface. The development of a surface analytical tool which probes the layer by layer composition of a bimetallic surface covered by an adsorbate would be of great benefit in understanding complex catalytic and corrosion processes. This paper examines critically the possibility of using medium energy ion scattering to obtain such information. The unique shadowing and blocking capabilities of this technique make it possible, in principle, to selectively illuminate integer numbers of surface layers. As the physics of the incident ion-surface atom collision is well established, it should then be possible to effectively count the number of each atom type present in the first layer, the top two layers, the top three layers, etc., of the bimetallic surface, thereby giving quantitative compositional information. Using a combination of experiment and simulation, we investigate how the number of layers illuminated depends on the extent of the surface layer relaxation, the adsorbate and the surface Debye temperature. We calculate the layer compositions of the top three layers in the $Cu_{50}Pd_{50}(110)/C_2H_{4-x}Cl_x$ system. We show that hydrocarbon adsorption produces a measurable Pd enrichment in the surface layer, while Cu enrichment is produced by the presence of Cl(ads) and C(ads).

Introduction

The physical and chemical properties of bimetallic surfaces are of huge technological interest particularly in the design of bimetallic catalysts and in the investigation of surface corrosion.[1−3] It is well-known that the composition of a bimetallic surface may differ strongly from that of the bulk material, these differences being driven by a complex interplay of thermodynamic parameters such as relative surface energies, relative bonding strengths of each metallic component with adsorbed atoms and molecules, and the tendency of the metal components to form ordered alloy phases and kinetic parameters such as diffusion barriers. The quantitative analysis of the layer by layer composition of a bimetallic surface is a nontrivial analytical task. Such information can be extricated from X-ray photoelectron spectra (XPS) with some difficulty by utilizing the exponential dependence of the peak intensity on the inelastic mean free path of the photoelectrons. Recent advances in scanning tunneling microscopy (STM) have led to the possibility of chemical differentiation between atom types in bimetallic surfaces [e.g., Wouda et al., PtRh(100)],[4] which therefore gives a quantitative compositional analysis of the (clean) surface layer. In addition, the sensitivity of low energy ion scattering (LEIS) to the topmost surface layer has enabled surface compositional analysis. In conjunction with LEED I(V) analysis, LEIS data can be used to quantify the composition of the top few layers of a bimetallic surface as in the case of $Pt_{25}Rh_{75}$(110) and (111).[5]

The shadowing and blocking capabilities of medium energy ion scattering (MEIS) make this a unique technique for obtaining layer by layer depth profile information. However, to our knowledge, this technique has only been used by two groups to quantify the near surface composition of bimetallic surfaces. These studies investigated the $Fe_{72}Cr_{28}$(110) surface[6] and the $Pt_{50}Ni_{50}$(111) surface.[7] In addition, Deckers et al. investigated oxygen induced segregation in the $Pt_{50}Ni_{50}$(111) system.[8] These studies have essentially involved extremely accurate investigations on well-defined surfaces. In this manuscript we investigate the potential of MEIS as a technique for analyzing the layer by layer composition of surfaces covered by complex, possibly poorly defined, adsorbate layers. We have recently shown that it is possible to glean compositional information of the surface region even in the presence of complex adsorbate layers.[9] We have since examined every aspect of the theoretical simulations (VEGAS code)[10] in an attempt to improve the accuracy of our results. We consider how (i) the surface layer relaxation, (ii) the surface Debye temperature, and (iii) the presence of the adsorbate may effect the number of surface layers illuminated by the ion beam for each experimental geometry. We show that the surface Debye temperature is a crucial parameter. A model is employed whereby the vibrational enhancement decays exponentially with depth. Using this model, good agreement is achieved between the experimental data and the estimated layer yields. Having achieved this, we report how the layer compositions of the top four layers are affected subtly by the nature of the adsorbate. Under the thermal processing conditions used, little or no diffusion to the surface from >1 nm depth is

* To whom correspondence should be addressed. E-mail: cjb14@st-and.ac.uk. Fax: +44 1334 467285.

† Leverhulme Centre for Innovative Catalysis.

‡ Present address: School of Chemistry, University of St. Andrews, St. Andrews, United Kingdom; KY16 9ST.

§ Surface Science Research Centre.

|| Medium Energy Ion Scattering Facility.

10.1021/jp003227p CCC: $20.00
Published on Web 03/16/2001

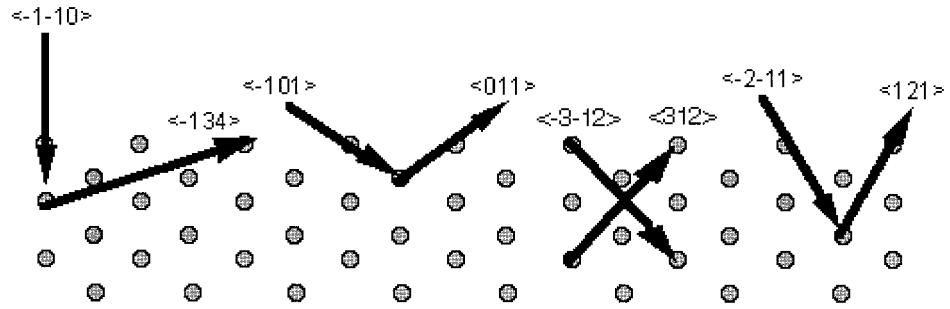

Figure 1. Cross sectional diagram of an fcc (110) surface viewed in the $\langle\bar{1}12\rangle$ azimuth. The incident and exit directions are labeled for one ($\langle\bar{1}01\rangle$ in, $\langle 011\rangle$ out), two ($\langle\bar{1}\bar{1}0\rangle$ in, $\langle\bar{1}34\rangle$ out); three ($\langle\bar{2}\bar{1}1\rangle$ in, $\langle 121\rangle$ out) and four ($\langle\bar{3}\bar{1}2>$ in, $\langle 132\rangle$ out) layer geometries.

detected—merely a swapping of Cu and Pd atoms between layers. We discuss how these changes are explained in terms of the known surface chemistry of ethene and 1,2-dichloroethene on Cu, Pd, and CuPd surfaces.

Experimental Section

Experimental data were collected using the Daresbury Laboratory MEIS facility.[11] This comprises an ion source and accelerator capable of producing H^+ or He^+ ions at energies up to 400 keV, a beamline for transport of the ions with a well-defined energy (<0.1%) and low angular divergence (<0.1°) and a multichamber ultrahigh vacuum (UHV) end station. The end station consists of a scattering chamber, a sample preparation and characterization chamber, a sample transfer system, and a fast entry load lock.

The scattering chamber contains a precision six axis goniometer to allow accurate alignment with the beam and a toroidal electrostatic energy analyzer with position sensitive detector to measure the scattered ion intensities as a function of scattering angle and energy. The detector system produces two-dimensional intensity maps of the ion intensity over a 1.8% range of pass energy and a scattering angle range of 24° with a resolution of 0.3% and 0.3°, respectively. Full two-dimensional data sets are accumulated by taking a series of "tiles" which cover the required angle/energy range and joining them together electronically to produce a single scattered ion intensity map. While two-dimensional data sets provide a complete picture of the scattering behavior, it is normal to process the data by integrating over a range of angles or energies to produce one-dimensional plots. Angle versus scattered ion intensity plots give structural information that can be used to calculate parameters such as surface layer relaxation. Energy spectra can be used to obtain quantitative compositional information, and a number of these plots are presented in this paper.

The preparation chamber contains facilities for argon ion bombardment cleaning and electron beam heating to enable clean well ordered surfaces to be prepared. Gas/vapor pressure dosing can be achieved via a precision leak valve. In addition, there are facilities for surface characterization: AES to determine composition and LEED to obtain information on long-range surface order. Samples can be transferred to the scattering chamber under ultrahigh vacuum conditions.

The $Cu_{50}Pd_{50}$(110) sample was sputtered at 573 K for 20 min, then cooled to 300 K while continuing the Ar^+ bombardment. The sample was then annealed to 923 K after which AES was used to detect any surface contamination and LEED showed a (1×1) structure. This sample preparation has been shown by Loboda-Cackovic to result in a disordered fcc surface.[12−14] Once clean, the sample was dosed with either *trans*-1,2-dichloroethene (DCE) or ethene and thermally processed where necessary prior to transfer (under UHV) to the MEIS chamber.

Data Analysis. *(1) Selection of Sample Geometries.* The Coulombic interaction between high-energy incident ions and the ion cores of the atoms in the solid lattice is such that shadow cones are produced which have, to a first approximation, the effect of shadowing any atoms which lie along the incident ion trajectory. We take advantage of this fact by choosing to align the sample along the incident directions shown in Figure 1. For example, ions travelling along incident direction $\langle\bar{2}11\rangle$ clearly strike all the atoms in each of the top three layers. However, the fourth and subsequent layers are shadowed from the incident beam and do not contribute to the scattered ion signal. As will be discussed in more detail below, there is a finite probability that atoms in deeper lying layers will be struck by the incident beam due to the fact that (i) lattice atoms are not fixed in space at 300 K (the analysis temperature) and vibrate with an amplitude related to the Debye temperature and (ii) the presence of the surface layer relaxation may expose underlying atoms to the beam (particularly in the 1 layer geometry). Therefore, to minimize the contribution to the signal from the lower lying layers, the ion intensity is measured along particular exit directions. Taking exit direction $\langle 121\rangle$ as an example, exiting ions from the top three layers can reach the detector, while ions which have collided with atoms from lower lying layers are unable to reach the detector as they are blocked by higher lying atoms. Ideally, this double alignment geometry ensures that using the incident and exit directions shown in Figure 1, we can selectively illuminate 1, 2, 3, and 4 layers of the surface. By measuring the actual number of Cu and Pd atoms struck by the incident beam for each geometry, we should therefore be able to calculate the composition of each of the top four layers. This forms the basis of our method, and is essentially a similar technique to that applied by Deckers et al. in the $Pt_{50}Ni_{50}$(111) system.[7,8]

(2) Data Processing. The MEIS data are acquired as functions of energy and scattering angle and an example is shown in Figure 2a. In this example, the low intensity channel at a scattering angle of 60° corresponds to the exit blocking direction $\langle 011\rangle$ in the 1 layer incident geometry. The ion intensity is summed over a narrow angular range at the base of the blocking channel resulting in the intensity v energy plot shown in Figure 2b. The peaks can be identified by using the following equation which is derived by assuming conservation of momentum and kinetic energy in a two-body collision.[15]

$$E_1/E_o = 1/(1 + A)^2[\cos\theta \pm (A^2 - \sin^2\theta)^{1/2}]^2 \qquad (1)$$

where E_1 is the energy of the peak, E_o is the incident beam energy, A is M_2/M_1 (where M_2 is the mass of the surface atom and M_1 is the mass of an impinging He atom), and θ is the scattering angle. (It is noteworthy that we are able to resolve peaks due to ^{35}Cl and ^{37}Cl using MEIS.) The intensities of the

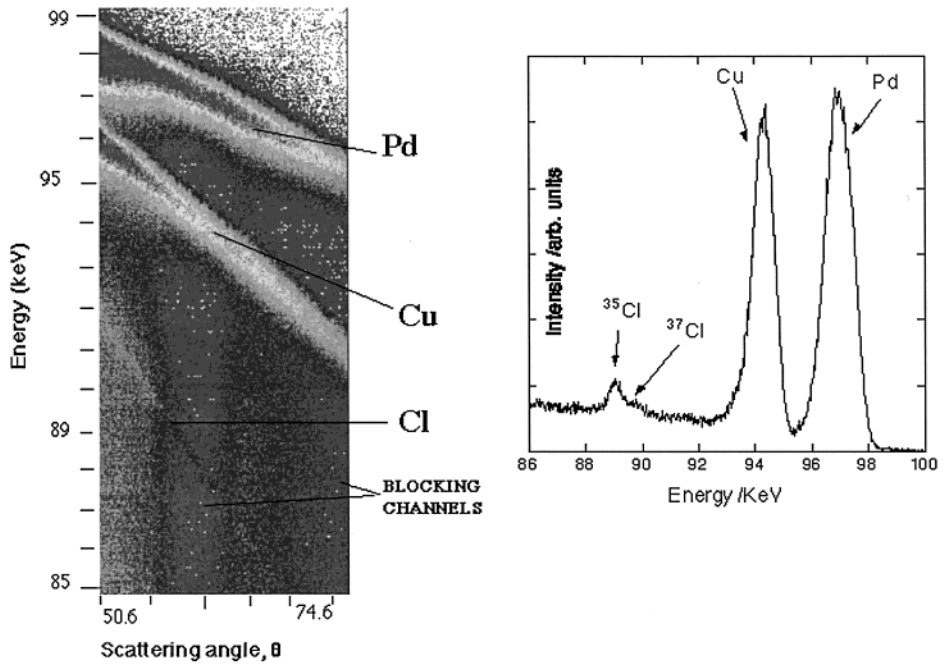

Figure 2. (a) Example of a typical MEIS data set showing ion intensity as a function of scattering angle and ion energy; (b) Example of a typical ion intensity vs ion energy plot achieved by integrating the data of Figure 2a along the ⟨011⟩ blocking direction.[9]

Cu and Pd peaks are measured by background subtraction and subsequent integration.

The probability density that an ion is scattered over a certain scattering angle is given by[16]

$$d\sigma/d\Omega = F[z_1 z_2 e^2/4E_o \sin^2(\theta/2)]^2 g(\theta,M_1,M_2) \qquad (2)$$

where F is the screening factor (arising from the Molière approximation) given by

$$F = 1 - (0.042 z_1 z_2^{4/3})/E_o \qquad (3)$$

and g is given by

$$g(\theta,M_1,M_2) \approx 1 - 2(M_1/M_2)^2 \sin^4\theta/2 \text{ for } M_1 \ll M_2 \qquad (4)$$

and z_1 and z_2 are the atomic numbers of the incident and target ions.

Both F and $g(\theta,M_1,M_2)$ are close to 1 in all our experiments. Therefore, to normalize the Cu and Pd peak areas such that for each experimental geometry the peak areas are directly proportional to a particular number of Cu and Pd atoms, we multiplied them by $[\cos(\phi) \sin^4(\theta/2)]/z_2^2$, where ϕ is the angle between the incident beam and the surface normal (the beam footprint correction). We carried out 14 separate experiments investigating the clean $Cu_{50}Pd_{50}(110)$ surface and the adsorption of DCE and ethene. Taking the average of the sums of the normalized Cu and Pd peaks for each geometry, we find values (arbitrary units) of 1 layer, 0.268 ± 0.015 (i.e., $\pm 5.6\%$); 2 layer, 0.365 ± 0.012 (i.e., $\pm 3.3\%$); 3 layer, 0.552 ± 0.019 (i.e., $\pm 3.5\%$); and 4 layer, 0.660 ± 0.037 (i.e. $\pm 5.6\%$) assuming the errors to be statistically derived and not systematic. This implies an approximate ratio of the layer illuminations of 1.0:1.36:2.05:2.46. These data imply that the double alignment geometry does not completely prevent the detection of ions scattered from lower lying layers. We therefore require some means of estimating the actual layer illumination for each geometry.

It is constructive to examine individually the experimental geometries and consider, in each case, the likelihood that there will be a contribution from deeper lying layers to the scattered ion signal.

(i) Shadow Cone Radius. The shadow cone radius at a distance d behind an atom of atomic number z_2 for a beam consisting of ions of atomic number z_1 and energy E is given by[16]

$$r_s = 2(z_1 z_2 e^2 d/4\pi\epsilon_o E)^{1/2} \qquad (5)$$

In the 1 layer geometry the beam is incident along the $\langle\bar{1}01\rangle$ direction. The second atom in the chain lies a distance $0.71a$ behind the first atom (where a is the lattice parameter of the fcc unit cell). In the 2 layer geometry, the beam is incident along the $\langle\bar{1}\bar{1}0\rangle$ direction (i.e., the surface normal). As in the 1 layer case, he second atom in the chain lies a distance $0.71a$ behind the first atom. In the 3 layer geometry, the beam is incident along the $\langle\bar{2}\bar{1}1\rangle$ direction and the second atom in the chain is now a distance $1.23a$ behind the first atom. In the 3 layer geometry, the shadow cone radius is ~30% larger at the second atom in the chain. Following similar arguments it can be shown that, in the 4 layer geometry, the shadow cone radius is ~62% larger than in either the 1 layer or the 2 layer cases. The undesired contribution to the scattered ion signal from deeper lying layers is expected to be diminished in the 3 layer geometry with respect to the 1 and 2 layer cases and is predicted to be negligible in the 4 layer geometry.

(ii) Surface Layer Relaxation. The presence of the surface layer relaxation is a second parameter that may cause unwanted illumination of deeper lying atoms. In the normal incidence geometry, the surface layer relaxation should have little effect on the number of layers illuminated by the beam. By contrast, the relatively grazing incidence geometry utilized for 1 layer illumination is much more sensitive to the surface layer relaxation. The use of double alignment geometry goes some way to quenching this effect, but the Cu and Pd peak areas are measured along the **bulk** exit direction, not the **surface** blocking direction. Therefore one might anticipate that the surface layer

relaxation will result in the illumination of considerably more than just the surface layer.

(iii) Enhanced Vibrations of Surface Atoms. The enhanced anisotropic vibrations of surface atoms will act to increase the numbers of illuminated layers. As this vibrational enhancement is largest in the *z* direction, this effect is expected to be most pronounced in the more grazing incident directions and much less noticeable in the normal incidence direction.

(iv) Effect of the Adsorbate. The primary motivation of this work is to develop a technique for the quantitative analysis of bimetallic surface composition **under the influence of the adsorbate**. It is extremely important therefore to consider the effect of the adsorbate on the layer illumination. Examination of the above equation for the shadow cone radius implies that Cl(ads) should be a relatively efficient shadowing atom (77% as effective as Cu, 61% as effective as Pd) and that the presence of Cl(ads) (in our experiments $0 < \Theta_{Cl} < 0.35$ ML) may therefore have a significant effect on the layer illumination. By contrast, C (ads) is a much less efficient shadower (45% as effective as Cu and 36% as effective as Pd). However, Cl (ads) will have a significant effect if it is either adsorbed in atop sites (where the effect would be strong in the normal incidence geometry) or if it adsorbed in a high symmetry site. Previous investigations of Cl adsorption on fcc(110) surfaces indicate that there are three possible binding sites on the (110) surface: 4-fold hollow sites directly atop second layer atoms, 2-fold hollow sites bridging two rows of top layer atoms, and pseudo 3-fold sites in the (111) microfacets on the trough edges. To our knowledge, no studies of chlorine adsorption on the Cu-(110) surface have been conducted to date. On Ag(110), low Cl coverages (<0.5 ML) produce a (2×1) structure. The chlorine atoms sit in the 4-fold hollows in the troughs, directly above second layer atoms. At saturation coverage (0.75 ML) the Cl atoms move along the Ag rows to form an incommensurate structure where they occupy the psuedo 3-fold sites and form a $c(2 \times 4)$ overlayer.[17−19] We have observed a $c(2 \times 4)$ LEED pattern following adsorption of molecular chlorine at room temperature and subsequent annealing to 475 K.[20] This may indicate that the (111) microfacet site is also occupied by the chlorine atoms on the $Cu_{50}Pd_{50}$(110) alloy surface. If this is the case, it is unlikely that shadowing by Cl(ads) will have a significant effect on the layer illuminations. Figure 3 shows the Cu + Pd normalized peak areas for the 2 layer geometry plotted against Cl coverage. It may be concluded that there is no downward trend in peak area as a function of Cl coverage which implies that Cl does not sit in an atop site. Also shown in Figure 3 are the normalized Cu+Pd peak intensities as a function of Cl coverage for the 1 layer geometry. There may be an indication that increasing Cl coverage causes a decrease the Cu + Pd peak intensity. Cl adsorption may be anticipated to alter the surface layer relaxation and damp the anisotropic enhanced vibrations of the surface atoms (this effect being largest perpendicular to the surface). Each of these changes would affect the 1 layer illumination much more strongly than those for the 2, 3, and 4 layer geometries. The data presented are derived from experiments where Cl_2 was dosed from an electrochemical source at 300 K. The coverage of Cl achieved by dosing 10 L DCE corresponds to ~0.15 ML. In this coverage regime, the 1 layer yield is close to that of the clean surface. Therefore, we chose to consider that layer illumination is unaffected by the presence of the adsorbate in any of our experiments. This conclusion is perhaps unexpected. One reason for the limited effect of Cl(ads) may be due to the vibrational amplitude of the adsorbed atom. Just as one would predict an increase in the layer illumination if the sample temperature was increased (i.e., due to the enhanced vibrations of Cu and Pd atoms), a strongly vibrating adsorbate atom would be a less efficient shadowing atom than a similar atom frozen in a particular lattice site.

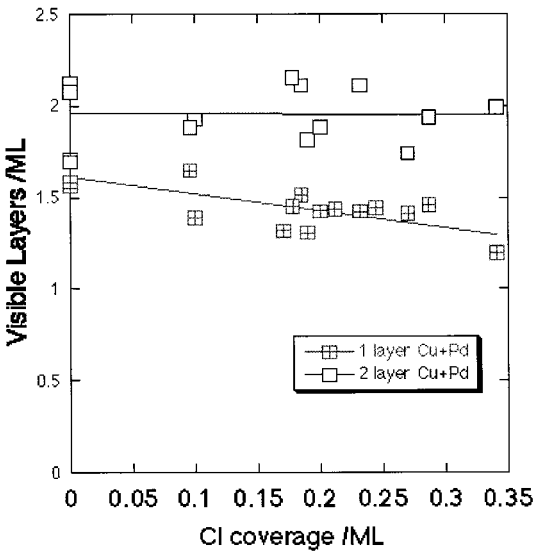

Figure 3. Variation of number of visible layers with Cl coverage for the 1 layer and 2 layer geometries. Data are taken from experiments involving the adsorption at 300 K of either molecular chlorine (from an electrochemical source) or dichloroethene onto $Cu_{50}Pd_{50}$(110).

The above discussion enables an empirical understanding of the likely number of illuminated layers for each experimental geometry. To select a particular range of values for the number of illuminated layers, we carried out simulations using the VEGAS code.[10] We now explain the models used and critically examine the output of the simulation program.

(3) VEGAS Simulations and Assumptions. The VEGAS code is well established as a means of analyzing MEIS data. Essentially, a starting structure was chosen which has the dimensions of the $Cu_{50}Pd_{50}$(110) lattice. The simplest way to model the effects of shadowing by lattice Cu and Pd atoms was to choose an atom with an atomic number midway between Cu(29) and Pd(46). Sr (atomic number 38) was chosen as the lattice atom for the model system. By comparison of the experimentally determined yields for each geometry between the alloy and pure Cu(110) we found this to be a valid approximation.

The second aspect of the theoretical model was the surface layer relaxation. By comparison of the angular position of the surface and bulk blocking dips in the experimental data for the 1 layer geometry, it would be possible to calculate the surface layer relaxation for each geometry. This relaxation could then be input into the VEGAS simulation. An idea of how dramatic one might anticipate the effect of the surface layer relaxation to be can be obtained by the following. If the beam is incident along $\langle\bar{1}01\rangle$ (1 layer incidence geometry) the second atom in the chain is ~2.6 Å behind the shadowing atom. If the latter atom is Cu, one may estimate the radius of the shadow cone at the second atom to be ~0.3 Å. A 10% surface layer relaxation (or contraction) is considered to be at the upper limit of the anticipated range even for the more open fcc(110) surface. The vertical displacement of the surface atom under these conditions would be ~0.21 Å (i.e., slightly less than the shadow cone radius at the second layer atom). Taking into account lattice vibrations, it is clear that the surface layer relaxation might be anticipated to cause some increase in the number of illuminated layers, but

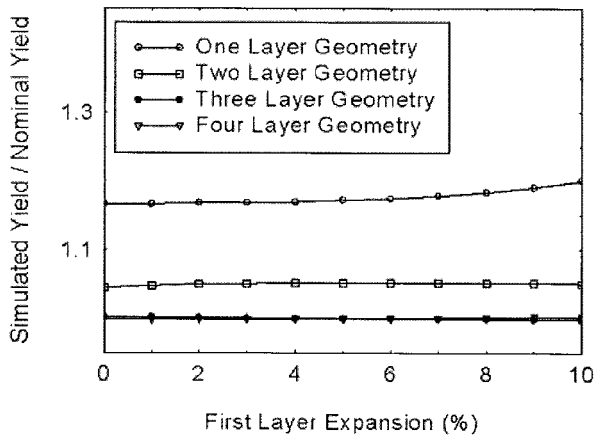

Figure 4. Variation in the predicted number of visible layers as a function of surface layer relaxation in the 1 layer geometry.

that this effect is likely to be small. This is supported by the data presented in Figure 4 which confirms that the variation in layer illuminations as a function of surface layer relaxation is relatively small over realistic values of the relaxation. The effect is further minimized as a consequence of the use of double alignment geometry which tends to remove the contribution of atoms exposed to the ion beam due to the surface layer relaxation.

Thermal vibrations of bulk atoms were taken into account by averaging the bulk Debye temperatures for Cu and Pd.

The surface vibrational enhancement emerged as the most critical parameter. One of the most difficult obstacles to overcome was the remarkably large range of literature values quoted for the surface Debye temperature of Cu(110). Literature values for the surface Debye temperature of Cu(110) range from 112 to 313 K depending on the orientation of the measurement.[21−27] These values can produce vibrational enhancements from 1.1 to 3.0, giving 1 layer geometry yields in the range 1.1 to 1.8. Many of these measurements are derived from ion scattering techniques. Interestingly, many of the lower values are derived for the $\langle\bar{1}12\rangle$ azimuth which is the azimuth of interest in this study. In addition, the only reported value for the surface Debye temperature of $Cu_{50}Pd_{50}(110)$ is 200−250 K.[28] Our initial VEGAS model allowed the surface atoms to vibrate with isotropically enhanced amplitudes, while all atoms below the surface vibrate with amplitudes characteristic of the bulk Debye temperature. To achieve predicted layer yields whose relative values were in agreement with our experimentally derived ratios, we needed to invoke a value of 3.0 for the surface/bulk vibrational enhancement which is characteristic of a surface Debye temperature at the low extreme of the literature values for Cu(110). We therefore sought to improve our model. Fowler and Barth[29] empirically determined that the decay of thermal vibrational enhancement on Cu(100) was exponential with depth, such that at a depth of one lattice spacing the vibrational enhancement was $1/e^2$ (13.5%) of that of the surface atom. Jiang et al.[30] used a decay of a factor of 2 between adjacent layers in their investigation of Cu(100). This model seems more reasonable than simply allowing the surface atoms to vibrate with enhanced amplitudes. In the case of the fcc(110) surface the second layer atoms are coordinated to 10 nearest neighbors rather than the desired 12. Therefore, it is reasonable to assume that these atoms will behave to an extent like surface atoms. Choosing an exponential decay in vibrational enhancement with depth such that the vibrational enhancement of the second layer is $1/e$ of that of the top layer and selecting a surface/bulk vibrational enhancement of 2.0 [which is in the middle of the values quoted for Cu(110)], we obtained good agreement in terms of the ratios of the yields between experiment and VEGAS simulation. We therefore chose to use the following values in all subsequent calculations: (i) 1 layer geometry → 1.45 layers − 1.0 × top layer, 0.42 × second layer, 0.03 × third layer; 0 × fourth layer; (ii) 2 layer geometry → 2.26 layers − 1.0 × top layer, 1.0 × second layer, 0.2 × third layer; 0.06 × fourth layer; (iii) 3 layer geometry → 3.15 layers − 1.0 × top layer, 1.0 × second layer, 1.0 × third layer; 0.15 × fourth layer; (iv) 4 layer geometry → 4.00 layers − 1.0 × top layer, 1.0 × second layer, 1.0 × third layer; 1.0 × fourth layer. As the distance of the second atom behind the target atom along the incident trajectory is increased the number of "extra" layers illuminated decreases due to the increase in radius of the shadow cone. Hence, in the 4 layer geometry, no "unwanted" illumination is predicted.

Experimentally, assuming the sample is correctly aligned, the quality of the data is such that we have a high degree of confidence in establishing the ratio $w_{Cu}/(w_{Cu} + w_{Pd})$ where w_{Cu}

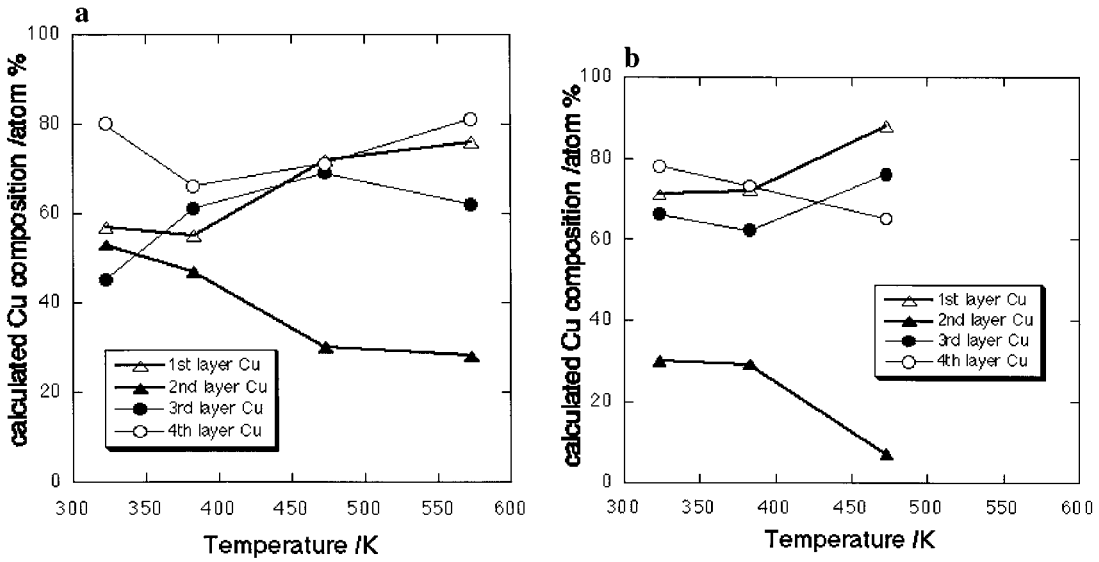

Figure 5. Variation in the composition of the top four layers of the $Cu_{50}Pd_{50}(110)$ surface as a function of temperature following the adsorption at 325 K of (a) ethene and (b) 1,2-dichloroethene.

TABLE 1

experiment	first layer (atom % Cu)	second layer (atom % Cu)	third layer (atom % Cu)	fourth layer (atom % Cu)
clean $Cu_{50}Pd_{50}$(110)	65	38	71	50
10 L ethene at 323 K	57	53	45	80
10L ethene at 323 K flashed to 383 K	55	47	61	66
10 L ethene at 323 K flashed to 473 K	72	30	69	71
10 L ethene at 323 K flashed to 573 K	76	28	62	81
10 L 1,2-dichloroethene at 323 K	71	30	66	78
10 L 1,2-dichloroethene at 323 K; flashed to 383K	72	29	62	73
10 L 1,2-dichloroethene at 323 K; flashed to 473 K	88	7	76	65
10 L 1,2-dichloroethene at 323 K; flashed to 573 K	data suggest surface restructuring			

and w_{Pd} are the normalized peak intensities for ions scattered from surface Cu and Pd atoms in the 1 layer illumination geometry. The product $1.45 \times w_{Cu}/(w_{Cu} + w_{Pd})$ gives the total number of Cu layers illuminated by the beam. This value is equal to $1.0a_{Cu} + 0.42b_{Cu} + 0.03c_{Cu} + 0d_{Cu}$ where a_{Cu}, b_{Cu}, c_{Cu}, and d_{Cu} are the fractional compositions of Cu in the top, second, third and fourth layers, respectively.

Similarly we may build up equations for the 2.26, 3.15, and 4.00 layer illuminations giving the following series of simultaneous equations:

$$1.0a_{Cu} + 0.42b_{Cu} + 0.03c_{Cu} + 0d_{Cu} = 1.45\, w_{Cu}/(w_{Cu} + w_{Pd})$$

$$1.0a_{Cu} + 1.0b_{Cu} + 0.20c_{Cu} + 0.06d_{Cu} = 2.26\, x_{Cu}/(x_{Cu} + x_{Pd})$$

$$1.0a_{Cu} + 1.0b_{Cu} + 1.0c_{Cu} + 0.15d_{Cu} = 3.15\, y_{Cu}/(y_{Cu} + y_{Pd})$$

$$1.0a_{Cu} + 1.0b_{Cu} + 1.0c_{Cu} + 1.0d_{Cu} = 4.00\, z_{Cu}/(z_{Cu} + z_{Pd})$$

and similar equations for w_{Pd} etc.

The solution of these equations is trivial and leads to the calculated values of the layer compositions for each of the top four layers. These values are summarized in Table 1.

Results and Discussion

To achieve a direct comparison between the experimental data and the theory we may normalize each set of data by the following procedures. We may divide the experimentally derived 1 layer value for the normalized Cu + Pd peak area (0.268 ± 0.015) by the sum of all the values from 1 to 4 layers and repeat for 2, 3, and 4 layers. Similarly for the theoretical data we can divide 1.45 (predicted value for the 1 layer illumination) by the sum of all four predicted values and repeat for the 2, 3, and 4 layer values. The following set of results is obtained:

	experiment	theory
1 layer	0.145 ± 0.016	0.133
2 layer	0.198 ± 0.020	0.208
3 layer	0.299 ± 0.030	0.290
4 layer	0.358 ± 0.039	0.369

Clearly, there is good agreement between the theoretical model and the experimental data.

The calculated values for each experimental system are presented in Table 1. The value for the clean surface layer composition (65%) is in good agreement with the value of 70% quoted by Bertolini and co-workers[31] and Loboda-Cackovic and co-workers[12−14] for similar sample preparation conditions. By contrast, the individual layer compositions vary dramatically depending on adsorbate and thermal processing. Figure 5, panels a and b, shows how the composition of each layer varies with these parameters. In each case it is clear that, to a first approximation, changes in the top layer composition are mirrored by changes in the opposite direction in the second layer. In addition, the overall composition of the top four layers changes little despite the range of experimental conditions employed. We find that this surface region is always slightly enriched in Cu (between ~56 and ~62%). The changes in surface composition can be assigned, therefore, to swapping of atoms between layers rather than a diffusion of material from the bulk of the sample.

The adsorption of ethene at 325 K causes a measurable decrease in the surface layer Cu content from 65 to 57%, which is maintained following the 383 K annealing treatment. Ethene does not adsorb under these conditions on Cu(110). On Pd(110), ethene adsorption at 300 K occurs dissociatively to form an ethynyl species (CCH) on the surface.[32] It, therefore, seems reasonable to propose that on the CuPd alloy dissociative ethene adsorption occurs at 323 K on small Pd ensembles, pinning Pd atoms into the surface layer. The higher heat of adsorption of ethene/ethynyl on Pd compared to Cu provides a driving force for Pd segregation, increasing the top layer Pd concentration, while decreasing the second layer Pd concentration. It appears that the third and fourth layers also respond to this effect dramatically, with their respective compositions swapping from Cu-rich to Pd-rich and from $Cu_{50}-Pd_{50}$ to Cu-rich, respectively, in response to the composition changes in the top two layers. On annealing the ethene covered surface to >473 K, the top layer Cu composition increases and surpasses the clean surface composition. By these temperatures ethynyl is known to decompose on Pd(110) to yield C(ads) and H_2(g).[32] It would, therefore, appear that while C_yH_x species cause Pd segregation into the surface layer, the presence of C(ads) has the opposite effect and results in a top layer Cu enhancement.

To explain the trends in layer composition caused by DCE we turn to the known chemistry of this molecule on Cu(110)[33] and Pd(110) surfaces.[34] On Cu(110), DCE dehalogenates upon adsorption to produce adsorbed chlorine and an acetylene species on the surface at 230 K. By 300 K, the acetylene has trimerised to form benzene which is then evolved into the gas phase at 370 K. No chlorinated desorption products are observed and a stable chlorinated surface is produced up to 550 K.[33] Molecular beam experiments show that the Pd(110) surface exhibits a more complex chemistry, governed by reactant uptake on the surface and activation energy barriers to product desorption.[34] Initially, at 300 K total decomposition of the DCE occurs, with desorption of H_2 into the gas phase. Carbon and chlorine laydown then poisons further C−C and C−H bond cleavage, leading to the formation of an acetylene species on the surface. Evolution of acetylene and HCl into the gas phase occurs at temperatures above 390 K, when the activation energy barrier to desorption can be overcome. Recent work,[35] suggests that the reaction of DCE on the CuPd(110) alloy is a combination of Cu and Pd chemistry. While the surface chemistry of the reactant tracks the events that occur on the Pd(110) surface, the evolution of

products into the gas phase is affected by the presence of the Cu with which Cl preferentially bonds. This leads to the following effects: HCl(g) production is halted and the Pd ensembles are kept relatively Cl-free so that acetylene interaction with the surface is not poisoned, allowing decomposition pathways to be preferred over desorption pathways. At 473 K, C(ads) and Cl(ads) are the species present on the CuPd surface. Under these conditions, the Cu concentration in the surface layer reaches a value of 88% while the second layer is strongly depleted in Cu (7%). C(ads) and Cl(ads) each cause the segregation of Cu to the surface layer.

Finally, following the anneal to 573 K the MEIS data showed an anomalously high background, indicative of restructuring of the CuPd(110) surface. This is possibly caused by the presence of $CuCl_x$ islands on the surface. Such Cl induced restructuring has been reported for Cl_2 adsorption on Ag(110).[36]

Conclusions

We have developed a fast an adaptable method of probing adsorbate induced segregation effects with MEIS. The critical parameter which must be modeled accurately to obtain meaningful results is the surface vibrational enhancement. In particular, it is important to allow the surface vibrational enhancement to exponentially decrease with depth.

We are able to determine the layer compositions of bimetallic single-crystal surfaces under the influence of complex adsorbates using a combination of experimental data and theoretical simulations.

C_xH_y hydrocarbons such as ethynyl lead to Pd segregation, while C(ads) and Cl(ads) lead to Cu-segregation. Therefore, these different adsorbate responses lead to interesting segregation balances, both as the nature of the reactant is altered (ethene versus dichloroethene) and as the surface chemistry changes with temperature.

The segregation processes induced by adsorption are localized to the top few layers of the surface. Under the experimental conditions used in this study, there is no sizable diffusion of one element to the surface from depths >1 nm.

Acknowledgment. We thank the Engineering and Physical Sciences Research Council (EPSRC) for the award of MEIS facility time (allocation periods MAP3-01 and MAP4-03). We are grateful to Professor Jean-Claude Bertolini for the loan of the $Cu_{50}Pd_{50}$(110) crystal. L.H.B. and S.C.L. acknowledge the award of an EPSRC CASE studentship with industrial sponsorship from ICI Chlorchemicals (Runcorn, UK).

References and Notes

(1) Rodriguez, J. A. *Surf. Sci. Rep.* **1996**, *24*, 225.
(2) Goodman, D. W. *Surf. Sci.* **1994**, *300*, 834.
(3) Campbell, C. T. *Annu. Rev. Phys. Chem.* **1990**, *41*, 775.
(4) Wouda, P. T.; Nieuwenhuys, B. E.; Schmid, M.; Varga, P. *Surf. Sci.* **1996**, *359*, 17.
(5) Platzgummer, E.; Sporn, M.; Koller, R.; Forsthuber, S.; Schmid, M.; Hofer, W.; Varga, P. *Surf. Sci.* **1999**, *419*, 236.
(6) Xu, C.; O'Connor, D. J. *Nucl. Instr. Methods Phys. Res. Sect. B* **1991**, *53*, 326.
(7) Deckers, S.; Habraken, F. H. P. M.; van der Weg, W. F.; van der Gon, A. W. D.; Pluis, B.; van der Veen, J. F.; Baudoing. R. *Phys. Rev. B* **1990**, *42*, 3253.
(8) Deckers, S.; Habraken, F. H. P. M.; van der Weg, W. F.; van der Gon, A. W. D.; van der Veen, J. F.; Geus, J. W. *Appl. Surf. Sci.* **1990**, *45*, 121.
(9) Baddeley, C. J.; Bloxham, L. H.; Laroze, S. C.; Raval, R.; Noakes, T. C. Q.; Bailey, P. *Surf. Sci.* **1999**, *433*−*435*, 827.
(10) Frenken, J. W. M.; Tromp, R. M.; van der Veen, J. F. *Nucl. Instr. Method B* **1986**, *17*, 334.
(11) Bailey, P.; Noakes, T. C. Q.; and Woodruff, D. P. *Surf. Sci.* **1999**, *426*, 358.
(12) Loboda-Cackovic, J.; Mousa, M. S.; Block, J. H. *Vacuum* **1995**, *46*, 89.
(13) Loboda-Cackovic, J. *Vacuum* **1997**, *48*, 1405.
(14) Loboda-Cackovic, J. *Vacuum* **1997**, *48*, 571.
(15) Woodruff, D. P.; Delchar, T. A. *Modern Techniques of Surface Science*; 2nd ed.; Cambridge University Press, 1994.
(16) Tromp, R. M. in *Practical Surface Analysis*, 2nd ed.; Briggs, D., Seah, M. P., Eds.; J. Wiley & Sons: Chichester, 1990; Vol. 2, pp 577−612.
(17) Bowker, M.; Waugh, K. C. *Surf. Sci.* **1985**, *155*, 1.
(18) Winograd, N.; Chang, C. C. *Phys. Rev. Lett*. **1989**, *62*, 2568.
(19) Moon, D. W.; Bleiler, R. J.; Winograd, N. *J. Chem. Phys.* **1986**, *85*, 1097.
(20) Bloxham, L. H.; Laroze, S. C.; Raval R.; Noakes, T. C. Q.; Bailey, P.; Baddeley, C. J. Manuscript in preparation.
(21) Jackson, D. P. *Surf. Sci.* **1974**, *43*, 431.
(22) Devyatko, Y. N.; Rogozhkin, S. V.; Troyan, V. I.; Gusev, E. P.; Gustafsson, T. *J. Exp. Theor. Phys.* **1999**, *89*, 1103.
(23) Durr, H.; Schneider, R.; Fauster, T. *Vacuum* **1990**, *41*, 376.
(24) Schneider, R.; Durr, H.; Fauster, T.; Dose, V. *Phys. Rev. B* **1990**, *42*, 1638.
(25) Fauster, T. *Vacuum* **1988**, *38*, 129.
(26) van de Riet, E.; Fluit, J. M.; Niehaus, A. *Vacuum* **1990**, *41*, 372.
(27) Speller, S.; Parascandola, S.; Heiland, W. *Surf. Sci.* **1997**, *383*, 131.
(28) Loboda-Cackovic, J. *Vacuum* **1995**, *46*, 1449.
(29) Fowler, D. E.; Barth, J. V. *Phys. Rev. B* **1995**, *52*, 2117.
(30) Jiang, Q. T.; Fenter, P.; Gustaffson, T. *Phys. Rev. B* **1991**, *44*, 5773.
(31) Rochefort, A.; Abon, M.; Delichère, P.; Bertolini, J. C. *Surf. Sci.* **1993**, *294*, 43.
(32) Yoshinobu, J.; Sekitani, T.; Onchi, M.; Nishijima, M. *J. Electron Spectrosc. Relat. Phenom.* **1990**, *54*, 697.
(33) Jugnet, Y.; Prakash, N. S.; Bertolini, J. C.; Laroze, S. C.; Raval, R. *Catal. Lett.* **1998**, *56*, 17.
(34) Bloxham, L. H.; Haq S.; Mitchell, C.; Raval, R. *J. Chem. Phys.* (manuscript submitted for publication).
(35) Bloxham, L. H.; Haq S.; Mitchell, C.; Raval, R. Manuscript in preparation.
(36) Andryushechkin, B. V.; Eltsov, K. N.; Shevlyuga, V. M. *Surf. Sci.* **1999**, *433*−*435*, 109.
(37) Laroze, S. C.; Haq. S.; Raval, R. Manuscript in preparation.